

COMPUTING THE RIEMANNIAN LOGARITHM ON THE STIEFEL MANIFOLD: METRICS, METHODS AND PERFORMANCE

RALF ZIMMERMANN* AND KNUT HÜPER†

Abstract. We address the problem of computing Riemannian normal coordinates on the real, compact Stiefel manifold of orthogonal frames. The Riemannian normal coordinates are based on the so-called Riemannian exponential and the Riemannian logarithm maps and enable to transfer almost any computational procedure to the realm of the Stiefel manifold. To compute the Riemannian logarithm is to solve the (local) geodesic endpoint problem. Instead of restricting the consideration to geodesics with respect to a single selected metric, we consider a family of Riemannian metrics introduced by Hüper, Markina and Silva-Leite that includes the Euclidean and the canonical metric as prominent examples.

As main contributions, we provide (1) a unified, structured, reduced formula for the Stiefel geodesics for the complete family of metrics, (2) a unified method to tackle the geodesic endpoint problem, (3) an improvement of the existing Riemannian log map under the canonical metric. The findings are illustrated by means of numerical examples, where the novel algorithms prove to be the most efficient methods known to this date.

Key words. Stiefel manifold, Riemannian logarithm, geodesic endpoint problem, Riemannian computing

AMS subject classifications. 15A16, 15B10, 33B30, 33F05, 53-04, 65F60

1. Introduction. As a rule, the practical execution of any data processing method on a curved manifold \mathcal{M} necessitates to work in local coordinates. This holds among others for basic tasks like averaging, clustering, interpolation and optimization. Of special importance are the *Riemannian normal coordinates*, as they are *radially isometric* [22, Lem. 5.10 & Cor. 6.11]. The Riemannian normal coordinates rely on the *Riemannian exponential* and the *Riemannian logarithm*, which are local diffeomorphisms: The exponential at a manifold location $p \in \mathcal{M}$ sends a tangent vector v (i.e. the velocity vector of a manifold curve) to the endpoint $q = c(1)$ of a geodesic curve c that starts from $p = c(0)$ with velocity $v = \dot{c}(0)$. The Riemannian logarithm at p maps a manifold location $q \in \mathcal{M}$ to the starting velocity vector v of a geodesic c that connects $p = c(0)$ and $q = c(1)$. Figure 1 illustrates this process. Hence, the Riemannian logarithm is associated with the

“Geodesic endpoint problem”: Given two manifold locations $p, q \in \mathcal{M}$, find a geodesic arc that connects p and q .

The Riemannian exponential and logarithm are important both from a theoretical perspective as well as in practical applications. Examples range from data analysis and signal processing [13, 28, 29] over computer vision [4, 24] to adaptive model reduction and subspace interpolation [5, 43], solving differential equations on manifolds [19, 9] and, more generally speaking, optimization techniques on manifolds [12, 1, 2]. This list is far from being exhaustive.

In this work, we tackle the geodesic endpoint problem on the Stiefel manifold of orthonormal frames. Geodesics depend on the way velocity vectors of curves are measured and thus on the Riemannian metric. Popular choices for metrics on the Stiefel manifold are the *Euclidean metric* and the *canonical metric*. These will be detailed in Section 2. Rather than restricting the considerations to either of these

*Department of Mathematics and Computer Science, University of Southern Denmark (SDU) Odense, (zimmermann@imada.sdu.dk)

†Institute of Mathematics, Mathematical Physics, Würzburg University, (hueper@mathematik.uni-wuerzburg.de)

two, we work with the one-parameter family of metrics that is introduced in [17]. This family contains the Euclidean and the canonical Stiefel metric as special cases.

Original contributions.

- We start from the results of [12] and [18] and derive a unified form for the Stiefel geodesics and thus for the Stiefel exponential. This form works for all metrics in the one-parameter family under consideration. Moreover it features the same structure as exhibited by the canonical geodesics and comes at roughly the same computational costs.
- We provide new theoretical insights on the structure of the matrices that come into consideration as candidate solutions for the Stiefel geodesic endpoint problem. For rectangular frames of dimensions $(n \times p)$, $n \gg p$, this reduces the endpoint problem essentially to finding suitable $(p \times p)$ -rotation matrices.
- We provide efficient algorithms for computing the Riemannian logarithm in a unified way for the full one-parameter family of metrics of [17]. The schemes are faster than all methods proposed in the literature up to now.
- For the special case of the canonical metric, the endpoint problem features a simplified structure that was exploited in [40]. We refine this approach and thus accelerate the existing method.
- We juxtapose the various methods by means of numerical experiments.

Related work. Literature on computing the Riemannian logarithm on the Stiefel manifold is sparse. The reference [29, section 5] tackles the geodesic endpoint problem for the canonical metric via a Riemannian optimization approach; [40] also works in the setting of the canonical metric and provides a matrix-algebraic algorithm based on the Baker-Campbell-Hausdorff formula with guaranteed local linear convergence. An algorithm for computing the Stiefel logarithm for the Euclidean metric is considered in [8] and is based on the general “shooting method”, see [34, section 6.5]. An algorithm for computing global Stiefel geodesics that is based on the “leapfrog method” of [27] for general manifolds is analysed in [36]. This approach requires local methods as building blocks.

Notational specifics. The $(p \times p)$ -identity matrix is denoted by $I_p \in \mathbb{R}^{p \times p}$, or simply I , if the dimension is clear. The $(p \times p)$ -orthogonal group, i.e., the set of all square orthogonal matrices is denoted by

$$O(p) = \{\phi \in \mathbb{R}^{p \times p} \mid \phi^T \phi = \phi \phi^T = I_p\}.$$

The standard matrix exponential and matrix logarithm are denoted by

$$\exp_m(X) := \sum_{j=0}^{\infty} \frac{X^j}{j!}, \quad \log_m(I + X) := \sum_{j=1}^{\infty} (-1)^{j+1} \frac{X^j}{j}.$$

The symmetric and skew-symmetric $(p \times p)$ -matrices are $\text{sym}(p) = \{A \in \mathbb{R}^{p \times p} \mid A^T = A\}$ and $\text{skew}(p) = \{A \in \mathbb{R}^{p \times p} \mid A^T = -A\}$, respectively.

When we employ the QR-decomposition of a rectangular matrix $A \in \mathbb{R}^{n \times p}$, we implicitly assume that $n \geq p$ and refer to the ‘economy size’ qr-decomposition $A = QR$, with $Q \in \mathbb{R}^{n \times p}$, $R \in \mathbb{R}^{p \times p}$.

2. The Stiefel manifold. This section reviews the essential aspects of Stiefel manifolds in regards of numerical, matrix-algorithmic applications. For additional background, see [12, 2, 41]. For featured applications, see [6, 10, 16, 38].

The *Stiefel manifold* $St(n, p)$ is the set of rectangular, column-orthogonal n -by- p matrices,

$$St(n, p) := \{U \in \mathbb{R}^{n \times p} \mid U^T U = I_p\} \subset \mathbb{R}^{n \times p}, \quad p \leq n.$$

Observe that this matrix set is a regular pre-image $St(n, p) = F^{-1}(0)$ of the function $F : \mathbb{R}^{n \times p} \rightarrow \text{sym}(p), Y \mapsto Y^T Y - I_p$. As such, it is a differentiable manifold of dimension $np - \frac{1}{2}p(p+1)$.

The *tangent space* $T_U St(n, p)$ at $U \in St(n, p)$ is

$$T_U St(n, p) = \{ \Delta \mid U^T \Delta \in \text{skew}(p) \} \subset T_U \mathbb{R}^{n \times p} \cong \mathbb{R}^{n \times p}.$$

For brevity, we will often write T_U instead of $T_U St(n, p)$. Every tangent vector $\Delta \in T_U$ may be written as

$$\begin{aligned} (1) \quad \Delta &= UA + (I - UU^T)T, & A \in \mathbb{R}^{p \times p} \text{ skew}, \quad T \in \mathbb{R}^{n \times p} \text{ arbitrary}, \\ (2) \quad \Delta &= UA + U^\perp H, & A \in \mathbb{R}^{p \times p} \text{ skew}, \quad H \in \mathbb{R}^{(n-p) \times p} \text{ arbitrary}, \end{aligned}$$

where in the latter case, $U^\perp \in St(n, n-p)$ is an orthogonal completion such that $(U \ U^\perp) \in O(n)$. Any matrix $W \in \mathbb{R}^{n \times p}$ can be projected onto T_U by

$$(3) \quad \Pi_U(W) = W - U \text{sym}(U^T W), \quad \text{sym}(U^T W) = \frac{1}{2}(U^T W + W^T U),$$

see [12, eqs. (2.3), (2.4)]

In order to turn $St(n, p)$ into a *Riemannian manifold* [23], a metric, i.e., an inner product $\langle \cdot, \cdot \rangle_U$ with associated norm $\| \cdot \|_U = \sqrt{\langle \cdot, \cdot \rangle_U}$ on the tangent spaces T_U must be defined for all $U \in St(n, p)$. Given a metric, the length of a curve $C : [a, b] \rightarrow St(n, p)$ is $L(C) := \int_a^b \|\dot{C}(t)\|_{C(t)} dt$. Candidates for length-minimizing curves are called *geodesics* and are locally uniquely determined by an ordinary initial value problem when specifying a starting point $C(0)$ and a starting velocity $\dot{C}(0)$, [23, §6]. It is obvious that geodesics depend on the underlying Riemannian metric.

Geodesics give rise to the Riemannian exponential map. On the Stiefel manifold, the Riemannian exponential at a base point $U \in St(n, p)$ sends a Stiefel tangent vector Δ to the endpoint $C(1) = \tilde{U} \in St(n, p)$ of a geodesic $t \mapsto C_{U, \Delta}(t)$ that starts from $C(0) = U$ with velocity vector $\dot{C}(0) = \Delta$,

$$\text{Exp}_U(\Delta) = C_{U, \Delta}(1), \quad C_{U, \Delta}(t) = \text{Exp}_U(t\Delta).$$

Knowing the Riemannian exponential is knowing the geodesics and vice versa.

The Riemannian exponential is locally invertible. The inverse is called the *Riemannian logarithm* and is denoted

$$(4) \quad \text{Log}_U : St(n, p) \ni \tilde{U} \mapsto \text{Log}_U(\tilde{U}) := \text{Exp}_U^{-1}(\tilde{U}) \in T_U St(n, p).$$

More precisely, $\text{Log}_U(\tilde{U})$ is well defined for all \tilde{U} within the *injectivity radius* $r_{St}(U)$ of $St(n, p)$ at U . The injectivity radius at U is the Riemannian distance of U to its cut locus C_U . The cut locus, in turn, is the set of points beyond which the geodesics starting from U cease to be length-minimizing. The global injectivity radius is $r_{St} := \inf\{r_{St}(U) \mid U \in St(n, p)\} = \inf_{U \in St(n, p)} \{\text{dist}(U, C_U)\}$, see [11, p. 271]. Combined, the Riemannian logarithm and exponential provide the *Riemannian normal coordinates*, which allow to map data points back and forth between the curved manifold and the flat tangent space, see Figure 1. This is crucial for all data processing operations on manifolds (optimization, interpolation, averaging, clustering,...). The Riemannian normal coordinates are special in that they are length-preserving along geodesic rays; one speaks of radial isometries.

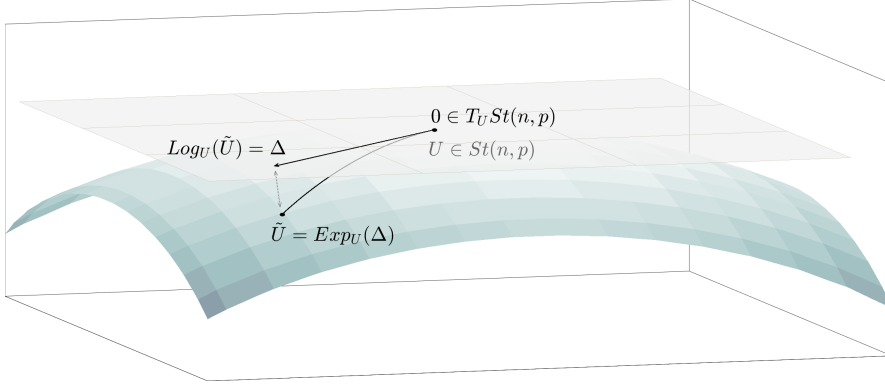


FIG. 1. Conceptual visualization of the Stiefel manifold $St(n, p)$ (curved surface) and associated tangent space $T_U St(n, p)$ (shaded plane). The Riemannian exponential sends a tangent vector Δ from $T_U St(n, p)$ to the endpoint \tilde{U} of the geodesic $C_{U, \Delta} : [0, 1] \rightarrow St(n, p)$ with initial values $C_{U, \Delta}(0) = U, C_{U, \Delta}'(0) = \Delta$. The Riemannian logarithm inverts this process.

The Euclidean and the canonical metric and generalizations. Let $U \in St(n, p)$ and let $\Delta = UA + U^\perp H$, $\tilde{\Delta} = U\tilde{A} + U^\perp \tilde{H} \in T_U$. Here and in the following, $A = U^T \Delta, \tilde{A} = U^T \tilde{\Delta} \in \text{skew}(p)$. There are two standard metrics on the Stiefel manifold.

The *Euclidean metric* on T_U is the one inherited from the ambient $\mathbb{R}^{n \times p}$:

$$\langle \Delta, \tilde{\Delta} \rangle_0 = \text{tr}(\Delta^T \tilde{\Delta}) = \text{tr} A^T \tilde{A} + \text{tr} H^T \tilde{H}.$$

The *canonical metric* on T_U is derived from the quotient representation $St(n, p) = O(n)/(O(n-p))$ of the Stiefel manifold and reads

$$\langle \Delta, \tilde{\Delta} \rangle_U = \text{tr} \left(\Delta^T \left(I - \frac{1}{2} U U^T \right) \tilde{\Delta} \right) = \frac{1}{2} \text{tr} A^T \tilde{A} + \text{tr} H^T \tilde{H},$$

see [12].

The Euclidean metric corresponds to measuring tangent vectors $\Delta = UA + U^\perp H$ in the Frobenius matrix norm

$$\sqrt{\langle \Delta, \Delta \rangle_0} = \|\Delta\|_F = \sqrt{\|A\|_F^2 + \|H\|_F^2} = \sqrt{2 \sum_{i < j} a_{ij}^2 + \sum_{i, j} b_{ij}^2},$$

while the canonical metric yields

$$\sqrt{\langle \Delta, \Delta \rangle_U} = \sqrt{\|\Delta\|_F^2 - \frac{1}{2} \|A\|_F^2} = \sqrt{\frac{1}{2} \|A\|_F^2 + \|H\|_F^2} = \sqrt{\sum_{i < j} a_{ij}^2 + \sum_{i, j} b_{ij}^2}.$$

In this sense, the Euclidean metric disregards the skew-symmetry of A and counts its individual entries a_{ij} twice, as was observed in [12, §2.4].

The work [17] recognizes the Euclidean and the canonical metric as special cases of a one-parameter family of inner products.

$$(5) \quad \langle \Delta, \tilde{\Delta} \rangle_U = \text{tr} \left(\Delta^T \left(I - \frac{2\alpha + 1}{2(\alpha + 1)} U U^T \right) \tilde{\Delta} \right) = \frac{1}{2(\alpha + 1)} \text{tr} A^T \tilde{A} + \text{tr} H^T \tilde{H},$$

for $\alpha \in \mathbb{R} \setminus \{-1\}$, where for $\alpha = -\frac{1}{2}$ and $\alpha = 0$, the Euclidean and the canonical metric are recovered, respectively.

Calculating the Riemannian Stiefel exponential: The state of the art.

A closed-form expression for the Stiefel exponential w.r.t. Euclidean metric is derived in [12, §2.2.2],

$$(6) \quad \tilde{U} = \text{Exp}_U^e(\Delta) = (U \quad \Delta) \exp_m \begin{pmatrix} A & -\Delta^T \Delta \\ I_p & A \end{pmatrix} \begin{pmatrix} I_p \\ 0 \end{pmatrix} \exp_m(-A).$$

In [18], an alternative formula is obtained:

$$(7) \quad \tilde{U} = \text{Exp}_U^e(\Delta) = \exp_m(\Delta U^T - U \Delta^T) U \exp_m(-A).$$

The advantage is that in this form, the Stiefel exponential features only standard matrix exponentials of skew-symmetric matrices. The downside is that $\Delta U^T - U \Delta^T \in \text{skew}(n)$ and working with $(n \times n)$ -matrices might be prohibitively expensive in large-scale applications, where $n \gg p$.

In [17], the formula (7) is generalized to the exponential for all α -metrics (5)

$$(8) \quad \tilde{U} = \text{Exp}_U^\alpha(\Delta) = \exp_m \left(-\frac{2\alpha + 1}{\alpha + 1} U A U^T + \Delta U^T - U \Delta^T \right) U \exp_m \left(\frac{\alpha}{\alpha + 1} A \right).$$

An algorithm for computing the Stiefel exponential w.r.t. the canonical metric was derived in [12, §2.4.2]: Given U, Δ , first compute a compact QR-decomposition $QR = (I - UU^T)\Delta$ with $Q \in St(n, p), R \in \mathbb{R}^{p \times p}$. Then form

$$(9) \quad \tilde{U} = \text{Exp}_U^c(\Delta) = (U \quad Q) \exp_m \begin{pmatrix} A & -R^T \\ R & 0 \end{pmatrix} \begin{pmatrix} I_p \\ 0 \end{pmatrix},$$

where again $A = U^T \Delta \in \text{skew}(p)$. This form is efficient, if $p < \frac{n}{2}$.

Calculating the Riemannian Stiefel logarithm: State of the art. Computing the Riemannian logarithm corresponds to solving the *geodesic endpoint problem* locally:

Given $U, \tilde{U} \in St(n, p)$ find a starting velocity $\Delta \in T_U$ such that

$$\text{Exp}_U(\Delta) = \tilde{U} \quad (\Leftrightarrow \Delta = \text{Log}_U(\tilde{U})).$$

An heuristic, generic method for solving the geodesic endpoint problem on any manifold is the shooting method, see [34, section 6.5]. This method is considered in [8] to compute the Stiefel logarithm. For the specific case of $St(4, 2)$ it features in [35]. The generic principle of the shooting method is as follows:

- find an initial guess $\Delta_0 \in T_U$.
- “shoot” a geodesic in the direction of Δ_0 , i.e., compute $\tilde{U}_0 := \text{Exp}_U(\Delta_0)$.
- measure the gap f_g between \tilde{U}_0 and the actual target \tilde{U} as a function of Δ .
- use information on the gap to update $\Delta_1 \leftarrow \Delta_0$ and repeat.

There are many options to detail the above steps. In [8], the initial guess is chosen as $\Delta_0 = \Pi_U(U - \tilde{U}) \in T_U$. The gap is measured in the ambient $\mathbb{R}^{n \times p}$ as $f_g(\Delta_0) = \|\tilde{U}_0 - \tilde{U}\|_F^2 = \|\text{Exp}_U(\Delta_0) - \tilde{U}\|_F^2$. A natural choice for updating the shooting direction Δ is a gradient descent based on this gap function. However, numerical computation of the gradient $\nabla(f_g)_\Delta$ requires in particular the derivative of the matrix exponential, which is expensive to obtain, see [15, Section 10.6] for the general formulas and [35, Prop.12], [42, Lem. 5] for precise applications to the Stiefel exponential. Therefore, [8] proposes to project the gap vector onto $T_{\tilde{U}}St(n, p)$ and to parallel-translate the result to $T_USt(n, p)$. This process is detailed in [Algorithm 1](#).

Algorithm 1 Shooting method, adapted from [8, Alg. 1]

Input: Stiefel matrices $U, \tilde{U} \in St(n, p)$, convergence threshold $\epsilon > 0$, time step array

$T = [t_0, t_1, \dots, t_m]$, with $t_0 = 0, t_m = 1.0$.

```

1:  $\nu \leftarrow \|\tilde{U} - U\|$ 
2:  $\Delta \leftarrow \nu \frac{\Pi_U(\tilde{U})}{\|\Pi_U(\tilde{U})\|}$       {project gap onto  $T_U$ , preserve the original length}
3: while  $\nu > \epsilon$  do
4:   for  $j = 1, \dots, m$  do
5:      $\tilde{U}^s(j) \leftarrow \text{Exp}_U(t_j \Delta)$       {discrete representation of geodesic}
6:   end for
7:    $\Delta^s \leftarrow \tilde{U}^s(m) - \tilde{U}$   {current gap vector: compare endpoint of geodesic to  $\tilde{U}$ }
8:    $\nu \leftarrow \|\Delta^s\|$ 
9:   for  $j = m, \dots, 0$  do
10:     $\Delta^s \leftarrow \nu \frac{\Pi_{\tilde{U}^s(j)}(\Delta^s)}{\|\Pi_{\tilde{U}^s(j)}(\Delta^s)\|}$   {initial projection plus approximate parallel transport}
11:  end for
12:  update  $\Delta \leftarrow \Delta - \Delta^s$ 
13: end while

```

Output: Δ

Note: The first inner iteration in the loop in steps 9-11 projects the gap vector of step 7 onto $T_{\tilde{U}^s(m)}$. The remaining steps realize an approximation of the parallel transport along the discretized geodesic $t \mapsto \text{Exp}_U(t\Delta)$.

A Stiefel log algorithm that is tailored for the canonical metric and features guaranteed local linear convergence is given in [40]. This approach will be explained and enhanced in [Subsection 3.4](#).

3. Fast computational schemes for solving the geodesic endpoint problem. In this section, we first prepare the grounds for a unified framework to tackle the geodesic endpoint problem. Then, we introduce practical numerical algorithms for computing the Stiefel logarithm, which improve on the state of the art in terms of the computational efficiency.

3.1. A reduced formula for the Stiefel exponential. As a starting point for efficient computational schemes, we derive an alternative expression for the α -metric Stiefel exponential that combines the advantages of (6) and (8) and represents a considerable computational reduction if $n \gg p$. To this end, assume that $p \leq \frac{n}{2}$. Let $U \in St(n, p)$ be given and take any suitable orthogonal extension $U^\perp \in St(n-p, p)$ such that $\Phi = (U \ U^\perp) \in O(n)$ is square and orthogonal. Observe that $\Phi^T U = \begin{pmatrix} I_p \\ 0 \end{pmatrix}$. With $\nu = \frac{2\alpha+1}{\alpha+1}, \mu = \frac{\alpha}{\alpha+1} = \nu - 1$, we rewrite (8):

$$\begin{aligned}
\text{Exp}_U^\alpha(\Delta) &= \Phi \Phi^T \exp_m(-\nu U A U^T + \Delta U^T - U \Delta^T) \Phi \Phi^T U \exp_m(\mu A) \\
&= \Phi \exp_m(-\nu \Phi^T U A U^T \Phi + \Phi^T (\Delta U^T - U \Delta^T) \Phi) \Phi^T U \exp_m(-A) \\
&= \Phi \exp_m \begin{pmatrix} -\nu A + U^T \Delta - \Delta^T U & -\Delta^T U^\perp \\ (U^\perp)^T \Delta & 0 \end{pmatrix} \begin{pmatrix} I_p \\ 0 \end{pmatrix} \exp_m(\mu A) \\
(10) \quad &= (U \ U^\perp) \exp_m \begin{pmatrix} (2-\nu)A & -H^T \\ H & 0 \end{pmatrix} \begin{pmatrix} I \\ 0 \end{pmatrix} \exp_m(\mu A), \quad H = (U^\perp)^T \Delta.
\end{aligned}$$

Let $H = \tilde{Q} \begin{pmatrix} B \\ 0 \end{pmatrix}$ with $\tilde{Q} = (\tilde{Q}_p \ \tilde{Q}_{n-2p}) \in O(n-p)$ a (full) QR-decomposition.

(Only the orthogonality of \tilde{Q} matters, B need not be triangular for the following considerations.)

We can factor

$$\begin{pmatrix} (2-\nu)A & -H^T \\ H & 0 \end{pmatrix} = \begin{pmatrix} I_p & 0 \\ 0 & \tilde{Q} \end{pmatrix} \exp_m \begin{pmatrix} (2-\nu)A & -B^T & 0 \\ B & 0 & 0 \\ 0 & 0 & 0 \end{pmatrix} \begin{pmatrix} I_p & 0 \\ 0 & \tilde{Q}^T \end{pmatrix},$$

which yields $\text{Exp}_U^\alpha(\Delta) = (U \ U^\perp \tilde{Q}_p) \exp_m \begin{pmatrix} (2-\nu)A & -B^T \\ B & 0 \end{pmatrix} \begin{pmatrix} \exp_m(\mu A) \\ 0 \end{pmatrix}$. Note that $U^\perp H = U^\perp (U^\perp)^T \Delta = (I - UU^T)\Delta$. Hence, instead of computing a QR-decomposition of $U^\perp H$, we can directly compute a compact QR-decomposition $QB = (I - UU^T)\Delta$ with $Q \in St(n, p)$ (Again, no special structure is required for $B \in \mathbb{R}^{p \times p}$.) This leads to the following proposition, which aligns in form and type with (9).

PROPOSITION 1. *Let $p \leq \frac{n}{2}$. For $U \in St(n, p)$, $\Delta \in T_U St(n, p)$ the Euclidean Stiefel exponential reads*

$$(11) \quad \text{Exp}_U^\alpha(\Delta) = (U \ Q) \exp_m \begin{pmatrix} \frac{1}{\alpha+1}A & -B^T \\ B & 0 \end{pmatrix} \begin{pmatrix} I_p \\ 0 \end{pmatrix} \exp_m \begin{pmatrix} \alpha \\ \alpha+1 \end{pmatrix} A,$$

where $A = U^T \Delta \in \text{skew}(p)$ and $QB = (I - UU^T)\Delta \in \mathbb{R}^{n \times p}$ is any matrix decomposition with $Q \in St(n, p)$ and $B \in \mathbb{R}^{p \times p}$.

As with (9), this form features only standard matrix exponentials of skew-symmetric matrices, whose dimensions scale in p rather than n . With Proposition 1, the Stiefel exponential is computable for all metrics in the α -family (5) in $\mathcal{O}(np^2)$ flops. A more detailed look on the calculations reveals that the formula (11) remains valid also if $p > \frac{n}{2}$. However, in this case, it represents in fact an increase in dimension for the main matrix exponential rather than a reduction when compared to (8). The formula (11) continues to hold if the orthogonal component $(I - UU^T)\Delta$ of the tangent vector is rank-deficient. In this case, it is understood that the QR-decomposition $QB = (I - UU^T)\Delta$ be arranged such that $QB = (Q_r \ Q_{p-r}) \begin{pmatrix} B_r \\ 0 \end{pmatrix}$, where $B_r \in \mathbb{R}^{r \times p}$ and $\text{rank}(B_r) = \text{rank}((I - UU^T)\Delta) = r$ and $B_r = 0$ in the extreme case of $0 = (I - UU^T)\Delta$.

Before we continue with the main body of this work, we note a curious aside.

LEMMA 2. *For $A \in \text{skew}(p)$, $H \in \mathbb{R}^{(n-p) \times p}$, it holds*

$$\begin{pmatrix} I_p & A \\ 0 & H \end{pmatrix} \exp_m \begin{pmatrix} A & A^2 - H^T H \\ I_p & A \end{pmatrix} \begin{pmatrix} I_p \\ 0 \end{pmatrix} = \exp_m \begin{pmatrix} 2A & -H^T \\ H & 0 \end{pmatrix} \begin{pmatrix} I_p \\ 0 \end{pmatrix}$$

Proof. Fix an orthogonal matrix $(U \ U^\perp) \in O(n)$ and construct $\Delta = UA + U^\perp H$. Then, the lemma is a consequence of the fact that both (6) and (10) with $\alpha = -\frac{1}{2}$ are valid expressions of the (unique) Stiefel matrix exponential $\text{Exp}_U^\alpha(\Delta)$ that satisfy the associated initial value problem, when parameterised as $t \mapsto \text{Exp}_U^w(t\Delta)$. \square

3.2. The Stiefel log matrix equations. We continue to work under the assumption that $p \leq \frac{n}{2}$ with the setting of $n \gg p$ in mind for practical big-data applications. In this section, we show that, in essence, computing the Stiefel logarithm for all α -metrics corresponds to solving a nonlinear matrix equation, where the unknown is a $2p \times 2p$ skew-symmetric matrix.

Let $U \in St(n, p)$ and let $\tilde{U} \in St(n, p)$ be within the injectivity radius $r_{St}(U)$ of $St(n, p)$ at U . Let $\Delta \in T_U$ be such that $\text{Exp}_U(\Delta) = \tilde{U}$. Then, \tilde{U} has a representation

$$\tilde{U} = UM + QN, \quad M, N \in \mathbb{R}^{n \times p}, M^T M + N^T N = I_p,$$

where $Q \in St(n, p)$ is the ‘ Q -factor’ of a compact QR-decomposition $QB = (I - UU^T)\Delta$. For the canonical metric, this is immediately clear from (9). For the full family of α -metrics, this follows from (11). More precisely, M, N form the first block column of an orthogonal matrix

$$(12) \quad \begin{pmatrix} M & X \\ N & Y \end{pmatrix} = \exp_m \begin{pmatrix} \frac{1}{\alpha+1}A & -B^T \\ B & 0 \end{pmatrix} \begin{pmatrix} \exp_m(\frac{\alpha}{\alpha+1}A) & 0 \\ 0 & I_p \end{pmatrix} \in SO(2p).$$

Recall $A = U^T \Delta \in \text{skew}(p)$ and that $\alpha = 0$ and $\alpha = -\frac{1}{2}$ reproduce the canonical and the Euclidean metric, respectively. For brevity, write again

$$\mu = \frac{\alpha}{\alpha+1}, \quad \alpha \neq -1.$$

Now, we aim at reversing the process and consider Δ as unknown. We can still obtain M and N from the given data points U, \tilde{U} via

$$M = U^T \tilde{U}, \quad QN = (I - UU^T)\tilde{U}.$$

For the latter equation, any matrix decomposition that represents $(I - UU^T)\tilde{U}$ via a ‘subspace factor’ Q with orthogonal columns and a corresponding ‘coordinates factor’ N is suitable in order to obey the constraint that M and N be blocks of an orthogonal matrix, i.e., $I = M^T M + N^T N$. This incorporates some ambiguity. If $(I - UU^T)\tilde{U}$ has full rank p , then Q and N are unique up to a rotation/reflection $\Phi \in O(p)$. More precisely, for $\tilde{Q}\tilde{N} = (I - UU^T)\tilde{U} = QN$, it holds $Q = \tilde{Q}\Phi, N = \Phi^T \tilde{N}$ with $\Phi = \tilde{Q}^T Q$. If $\text{rank}(I - UU^T)\tilde{U} = r < p$, then we may assume that

$$(13) \quad (I - UU^T)\tilde{U} = QN = (Q_r, Q_{p-r}) \begin{pmatrix} N_r \\ 0 \end{pmatrix},$$

where $Q_r \in St(n, r), Q_{p-r} \in St(n, p-r), N_r \in \mathbb{R}^{p \times r}$. This determines Q_r, N_r uniquely up to a rotation/reflection $\Phi_r \in O(r)$. Yet, the column block Q_{p-r} may be an arbitrary orthogonal extension.

Once Q, M, N are chosen and fixed, we can compute matrix blocks X_0, Y_0 such that they form an orthogonal completion $V = \begin{pmatrix} M & X_0 \\ N & Y_0 \end{pmatrix} \in O(2p)$. The restriction of the exponential map to the skew-symmetric matrices

$$\exp_m|_{\text{skew}(p)} : \text{skew}(p) \rightarrow SO(p)$$

is surjective [14, §. 3.11, Thm. 9]. Hence, (12) requires to select X_0, Y_0 such that $\det(V) = +1$.¹ Again, such a completion is not unique and it cannot be expected that the such found X_0, Y_0 align with the structure of (12). Yet, there is an orientation preserving orthogonal matrix $\Phi = \exp_m(C), C \in \text{skew}(p)$ such that $\begin{pmatrix} X_0 \\ Y_0 \end{pmatrix} \Phi = \begin{pmatrix} X \\ Y \end{pmatrix}$ is the sought-after completion. In summary, computing the Stiefel logarithm boils down to solving the following nonlinear matrix equation:

¹As an aside, this is why the example S1 from the supplements of [40] fails.

$$(14) \quad \text{solve } F \begin{pmatrix} A & -B^T \\ B & C \end{pmatrix} = \begin{pmatrix} M & X_0 \\ N & Y_0 \end{pmatrix}, \quad \text{for } F : \text{skew}(2p) \rightarrow SO(2p),$$

$$F \begin{pmatrix} A & -B^T \\ B & C \end{pmatrix} = \exp_m \begin{pmatrix} (1-\mu)A & -B^T \\ B & 0 \end{pmatrix} \begin{pmatrix} \exp_m(\mu A) & 0 \\ 0 & \exp_m(-C) \end{pmatrix}, \mu = \frac{\alpha}{\alpha+1}.$$

The sought-after tangent velocity is then $\Delta = UA + QB \in T_U$. It is worth mentioning that any ambiguity in Q has no impact on the final Δ , not even in the case where the component $(I - UU^T)\tilde{U}$ of \tilde{U} does not feature full rank. This is confirmed in the next theorem, which can be considered as a generalization of [40, Thm. 3.1].

THEOREM 3. *Let $U, \tilde{U} \in St(n, p)$ with $\text{dist}(U, \tilde{U}) < r_{St}(U)$ and let*

$$U^T \tilde{U} = M, \quad (I - UU^T)\tilde{U} = QN = \begin{pmatrix} Q_r & Q_{p-r} \end{pmatrix} \begin{pmatrix} N_r \\ 0 \end{pmatrix}, \quad r \leq p,$$

with $Q \in St(n, p)$ and $r = \text{rank}(N_r) = \text{rank}(N)$. Then $\Delta = \text{Log}_U(\tilde{U})$ features a representation

$$\Delta = UA + QB = UA + \begin{pmatrix} Q_r & Q_{p-r} \end{pmatrix} \begin{pmatrix} B_r \\ 0 \end{pmatrix}, \quad A \in \text{skew}(p), \quad B_r \in \mathbb{R}^{r \times p}.$$

Here, A, B are components of a skew-symmetric block matrix that solves (14).

Proof. Let $M, N = \begin{pmatrix} N_r \\ 0 \end{pmatrix} \in \mathbb{R}^{p \times p}$, with $N_r \in \mathbb{R}^{r \times p}$ of full rank r constructed as stated above. We can restrict the considerations to block extensions X_0, Y_0 to an orthogonal matrix of the form

$$V = \begin{pmatrix} M & X_0 \\ N & Y_0 \end{pmatrix} = \left(\begin{array}{c|c|c} M & X_r^0 & 0 \\ N_r & Y_r^0 & 0 \\ \hline 0 & 0 & I_{p-r} \end{array} \right) \in SO(2p),$$

where $X_r^0 \in \mathbb{R}^{p \times r}, Y_r^0 \in \mathbb{R}^{r \times r}$ are obtained, say, via the Gram-Schmidt method.

Let $\begin{pmatrix} A & -B^T \\ B & C \end{pmatrix}$ be a solution to (14) that preserves the above structure of V so that

in particular $\begin{pmatrix} X_r^0 & 0 \\ Y_r^0 & 0 \\ \hline 0 & I_{p-r} \end{pmatrix} \exp_m(C) = \begin{pmatrix} X_r & 0 \\ Y_r & 0 \\ \hline 0 & I_{p-r} \end{pmatrix}$. This entails $\exp_m(C) = \Phi =$

$\begin{pmatrix} \Phi_r & 0 \\ 0 & I_{p-r} \end{pmatrix} \in SO(p)$. Then, for all α -metrics, it holds with $\mu = \frac{\alpha}{\alpha+1}$ that

$$(15) \quad \log_m \left(\begin{pmatrix} M & X_r^0 & 0 \\ N_r & Y_r^0 & 0 \\ \hline 0 & 0 & I_{p-r} \end{pmatrix} \begin{pmatrix} \exp_m(-\mu A) & 0 & 0 \\ 0 & \Phi_r & 0 \\ \hline 0 & 0 & I_{p-r} \end{pmatrix} \right) = \begin{pmatrix} (1-\mu)A & -B^T \\ B & 0 \end{pmatrix}.$$

Because the matrix logarithm acts block-wise on block-diagonal matrices, the block structure of the matrix on the left hand side entails a corresponding block structure for the right-hand side of (15). In particular, necessarily $B = \begin{pmatrix} B_r \\ 0 \end{pmatrix}$ with $\text{rank}(B_r) = r$.

Now, define $\Delta = UA + Q_r B_r$ and apply the Stiefel exponential in forward mode to check if $\text{Exp}_U(\Delta) = \tilde{U}$. According to (11), the procedure requires to compute

$U^T \Delta = A$, as well as an orthogonal decomposition

$$(I - UU^T)\Delta = (\hat{Q}_r \quad \hat{Q}_{p-r}) \begin{pmatrix} \hat{B}_r \\ 0 \end{pmatrix}.$$

The matrix factors \hat{Q}_r and \hat{B}_r are not necessarily equal to Q_r and B_r , respectively. Yet, by construction, it holds $\hat{Q}_r \hat{B}_r = (I - UU^T)\Delta = (I - UU^T)Q_r B_r = Q_r B_r$. Since Q_r, \hat{Q}_r span the same column-space, $S := Q_r^T \hat{Q}_r$ is orthogonal and $\hat{Q}_r = Q_r S, \hat{B}_r = S^T B_r$. The Stiefel exponential produces

$$\begin{aligned} \text{Exp}_U(\Delta) &= (U \quad \hat{Q}_r \quad \hat{Q}_{p-r}) \exp_m \begin{pmatrix} (1-\mu)A & -\hat{B}_r^T & 0 \\ \hat{B}_r & 0 & 0 \\ 0 & 0 & 0 \end{pmatrix} \begin{pmatrix} \exp_m(\mu A) \\ 0 \\ 0 \end{pmatrix} \\ &= (U \quad \hat{Q}_r) \exp_m \begin{pmatrix} (1-\mu)A & -\hat{B}_r^T \\ \hat{B}_r & 0 \end{pmatrix} \begin{pmatrix} \exp_m(\mu A) \\ 0 \end{pmatrix} \\ &= (U \quad \hat{Q}_r S) \exp_m \begin{pmatrix} (1-\mu)A & -\hat{B}_r^T S \\ S^T \hat{B}_r & 0 \end{pmatrix} \begin{pmatrix} \exp_m(\mu A) \\ 0 \end{pmatrix} \\ &= (U \quad Q_r) \exp_m \begin{pmatrix} (1-\mu)A & -B_r^T \\ B_r & 0 \end{pmatrix} \begin{pmatrix} \exp_m(\mu A) \\ 0 \end{pmatrix} = (U \quad Q_r) \begin{pmatrix} M \\ N_r \end{pmatrix} = \tilde{U}, \end{aligned}$$

because of (15). \square

Remark 4 (The search space for the Stiefel log algorithm). For Stiefel points U and $\tilde{U} = \text{Exp}_U(\Delta)$ within the injectivity radius at U , [Theorem 3](#) shows that both the location \tilde{U} and the tangent vector Δ are in the same matrix space

$$(16) \quad \mathcal{S} = \{UV \mid V \in \mathbb{R}^{p \times p}\} \oplus \{QW \mid W \in \mathbb{R}^{p \times p}\} \subset \mathbb{R}^{n \times p}.$$

This fact can be exploited in numerical schemes for computing the Stiefel logarithm. A direct consequence is that any numerical algorithm can focus on finding the missing factors $A, B \in \mathbb{R}^{p \times p}$.

3.3. A p -shooting method tailored for the Stiefel logarithm. In this section, we customize the generic iterative shooting method of [Algorithm 1](#) for solving the geodesic endpoint problem. With large “tall-and-skinny” matrices and big data applications in mind, our contribution is to modify the required calculations such that the loop iterations are tailored for the use of (11) and (16) and work exclusively with $2p \times 2p$ matrices rather than with $n \times p$ matrices. This leads to considerable savings, if $n \gg p$.

Given $U, \tilde{U} \in St(n, p)$, the starting point is the representation $\tilde{U} = UU^T \tilde{U} + (I - UU^T)\tilde{U} = U\hat{M} + Q\hat{N}$, where $\hat{M} = U^T \tilde{U} \in \mathbb{R}^{p \times p}$ and $Q\hat{N} = (I - UU^T)\tilde{U} \in \mathbb{R}^{n \times p}$ is a compact QR-decomposition. The essential observation is that all iterates Δ, Δ^s of [Algorithm 1](#) actually remain in the matrix space \mathcal{S} of (16) that is spanned by the fixed U and Q . According to [Theorem 3](#) and [Remark 4](#), \mathcal{S} also contains the sought-after solution.

PROPOSITION 5. *Let $U, \tilde{U} \in St(n, p)$ and let $Q\hat{N} = (I - UU^T)\tilde{U} \in \mathbb{R}^{n \times p}$ be a compact QR-decomposition. All tangent matrices Δ produced iteratively by [Algorithm 1](#) and all the update matrices Δ^s that are the final outcome of one pass through the while-loop in [Algorithm 1](#) allow for a representation of the form*

$$\Delta = UA + QR, \quad \Delta^s = UA^s + QR^s, \quad A, A^s \in \text{skew}(p), R, R^s \in \mathbb{R}^{p \times p}.$$

Remark: It is important to emphasize that it is *the same* Q-factor that works for all the iterates Δ, Δ^s . This enables to restrict the update to the A - and R -factors. The intermediate matrices Δ^s under the while-loop are also contained in the matrix space \mathcal{S} of Remark 4, but they are of the form $\Delta^s = UX^s + QR^s$ with $X^s \notin \text{skew}(p)$ in general.

Proof. The initial Δ_0 is obtained from the projection

$$\begin{aligned}\Delta_0 &= \Pi_U(\tilde{U} - U) = \Pi_U(\tilde{U}) = U\hat{M} + Q\hat{N} - U \text{sym}(\hat{M}) \\ &= U \text{skew}(\hat{M}) + Q\hat{N} =: UA_0 + QR_0.\end{aligned}$$

The first update Δ^s is obtained by projecting the gap $\tilde{U}_0^s - U$ onto $T_{\tilde{U}}$ and then further onto T_U by following the geodesic ‘backwards in time’. At every time instant t , it holds

$$\tilde{U}^s(t) = \text{Exp}_U(t\Delta_0) = \begin{pmatrix} U & Q \end{pmatrix} \begin{pmatrix} M_t & X_t \\ N_t & Y_t \end{pmatrix} \begin{pmatrix} I_p \\ 0 \end{pmatrix} = UM_t + QN_t,$$

where $\begin{pmatrix} M_t & X_t \\ N_t & Y_t \end{pmatrix}$ is evaluated according to (12) with inputs $A = tA_0, B = tR_0$.

If any matrix of the form $W = UX + QY$ is projected onto the tangent space at any $UM_t + QN_t$, the result is

$$\begin{aligned}\Pi_{UM_t + QN_t}(W) &= U(X - M_t \text{sym}(M_t^T X + N_t^T Y)) + Q(Y - N_t \text{sym}(M_t^T X + N_t^T Y)) \\ &= UX^\Pi + QY^\Pi.\end{aligned}$$

Hence, all operations performed in Algorithm 1 take place in the matrix space $\mathcal{S} = \{UX + QY | X, Y \in \mathbb{R}^{p \times p}\}$ of (16). \square

With Proposition 5, the computational costs associated with the shooting method can be reduced considerably. This gives rise to Algorithm 2.

The subroutine $\text{Exp4Geo}(\hat{A}, \hat{B}, \text{metric})$ that appears in step 8 of Algorithm 2 corresponds to an evaluation of (12) and outputs the first block column of the resulting orthogonal matrix. This subroutine is the only step that depends on the chosen metric and thus makes the only difference when computing the Stiefel logarithm for the canonical, the Euclidean or any other α -metric.

The subroutine $\text{ParaTrans_pFactors}(M(t), N(t), A^s, R^s, \nu)$ that appears in step 13 of Algorithm 2 realizes an approximation of the parallel transport of $\Delta^s = UA^s + QR^s$ along the geodesic using the unique representation with the p -factors A^s, R^s . This subroutine is detailed in Algorithm 3. A numerical experiment that illustrates the performance of Algorithm 2 is in Section 4.

3.4. An improved algebraic Stiefel logarithm for the canonical metric.

Let $U, \tilde{U} = UM + QN \in St(n, p)$ with $M = U^T \tilde{U}, QN = (I - UU^T)\tilde{U}$ and an orthogonal completion $\begin{pmatrix} M & X_0 \\ N & Y_0 \end{pmatrix} \in SO(2p)$ as introduced in the previous sections. In [40], it has been shown that for solving (14) in the case of the canonical metric, it is sufficient to find $\Gamma \in \text{skew}(p)$ such that

$$(17) \quad \begin{pmatrix} 0 & I_p \end{pmatrix} \log_m \left(\begin{pmatrix} M & X_0 \\ N & Y_0 \end{pmatrix} \begin{pmatrix} I_p & 0 \\ 0 & \exp_m(\Gamma) \end{pmatrix} \right) \begin{pmatrix} 0 \\ I_p \end{pmatrix} = 0 \in \mathbb{R}^{p \times p}.$$

With $V = \begin{pmatrix} M & X_0 \\ N & Y_0 \end{pmatrix} = \exp_m \begin{pmatrix} A_0 & -B_0^T \\ B_0 & C_0 \end{pmatrix}$ and $W = \exp_m \begin{pmatrix} 0 & 0 \\ 0 & \Gamma \end{pmatrix}$, (17) requires to find Γ such that the lower p -by- p diagonal block of the matrix $\log_m(VW)$ cancels.

Algorithm 2 p-Shooting method

Input: Stiefel matrices $U, \tilde{U} \in St(n, p)$, convergence threshold $\epsilon > 0$, array $T = [t_0, t_1, \dots, t_m]$, $t_0 = 0, t_m = 1.0$ (discretized unit interval), metric parameter α .

- 1: $\hat{M} = U^T \tilde{U}$
- 2: $Q\hat{N} = \tilde{U} - U\hat{M}$ {compact QR-decomposition}
- 3: $\nu \leftarrow \sqrt{\|\hat{M} - I_p\|^2 + \|\hat{N}\|^2}$ {note $\tilde{U} - U = U(\hat{M} - I_p) + Q\hat{N}$ }
- 4: $A \leftarrow \frac{\nu \text{skew}(\hat{M})}{\sqrt{\|\text{skew}(\hat{M})\|^2 + \|\hat{N}\|^2}}, \quad R \leftarrow \frac{\nu \hat{N}}{\sqrt{\|\text{skew}(\hat{M})\|^2 + \|\hat{N}\|^2}},$
- 5:
- 6: **while** $\nu > \epsilon$ **do**
- 7: **for** $j = 1, \dots, m$ **do**
- 8: $\begin{pmatrix} M(t_j) \\ N(t_j) \end{pmatrix} \leftarrow \text{Exp4Geo}(t_j A, t_j R, \alpha)$ {cf. (12)}
- 9: **end for** {p-factor representation of geodesic $U^s(t_j) = UM(t_j) + QN(t_j)$ }
- 10: $A^s \leftarrow M(t_m) - \hat{M}, R^s \leftarrow N(t_m) - \hat{N}$ {p-factors of current gap vector}
- 11: $\nu \leftarrow \sqrt{\|A^s\|^2 + \|R^s\|^2}$
- 12: **for** $j = m, \dots, 0$ **do**
- 13: $[A^s, R^s] = \text{ParaTrans_pFactors}(M(t_j), N(t_j), A^s, R^s, \nu)$ {initial projection plus approximate parallel transport}
- 14: **end for**
- 15: update $A \leftarrow A - A^s, \quad R \leftarrow R - R^s$ {updated $\Delta = UA + QR$ }
- 16: **end while**

Output: $\Delta = UA + QR$

Algorithm 3 ParaTrans.pFactors: Map the tangent vector $\Delta = UA_1 + QR_1 \in T_{U_1}$ to the tangent space T_{U_2} , preserve the length

Input: $M_2, N_2, A_1, R_1 \in \mathbb{R}^{p \times p}$, $\nu > 0$
{here, M_2, N_2 represent $U_2 = UM_2 + QN_2 \in St(n, p)$, A_1, R_1 represent $\Delta = UA_1 + QR_1 \in T_{U_1}$ }

- 1: $S \leftarrow \text{sym}(M_2^T A_1 + N_2^T R_1)$
- 2: $A_2 = A_1 - M_2 S, R_2 = R_1 - N_2 S$
- 3: $l = \sqrt{\|A_2\|^2 + \|R_2\|^2}$
- 4: **if** $l > \epsilon$ **then**
- 5: $A_2 = \frac{\nu}{l} A_2, R_2 = \frac{\nu}{l} R_2$ {rescale to original length}
- 6: **else**
- 7: $A_2 = 0, R_2 = 0.$
- 8: **end if**

Output: A_2, R_2

This algorithm executes the same operation as in step 10 of [Algorithm 1](#) but on the representative $p \times p$ matrix factors.

The Baker-Campbell-Hausdorff (BCH) series for the matrix logarithm is

$$\begin{aligned} \log_m(VW) &= \log_m(V) + \log_m(W) + \frac{1}{2}[\log_m(V), \log_m(W)] \\ &+ \frac{1}{12}([\log_m(V), [\log_m(V), \log_m(W)]] + [\log_m(W), [\log_m(W), \log_m(V)]]) + \dots, \end{aligned}$$

see [31, §1.3, p. 22]. The algorithm [40, Alg. 1] and the associated convergence analysis rely on the fact that with the choice of $\Gamma_0 = -C_0$, the lower p -by- p block of $\log_m(VW)$ cancels up to terms of third order in the BCH series. The algorithm iterates on this observation and produces the sequence

$$(18) \quad \begin{pmatrix} A_{k+1} & -B_{k+1}^T \\ B_{k+1} & C_{k+1} \end{pmatrix} := \log_m \left(\exp_m \begin{pmatrix} A_k & -B_k^T \\ B_k & C_k \end{pmatrix} \exp_m \begin{pmatrix} 0 & 0 \\ 0 & \Gamma_k \end{pmatrix} \right),$$

with $\Gamma_k = -C_k$. It is guaranteed that $\|C_k\| \rightarrow 0$ for $k \rightarrow \infty$ at a linear rate as long as the input points U, \bar{U} are close enough.

In fact, up to commutator products of order three, the BCH series expansion of the lower diagonal block of $\log_m(V_kW)$ is

$$\begin{aligned} & C_k + \Gamma + \frac{1}{2}(C_k\Gamma - \Gamma C_k) \\ & + \frac{1}{12}(C_k^2\Gamma + \Gamma C_k^2 + C_k\Gamma^2 + \Gamma^2 C_k - (B_k B_k^T \Gamma + \Gamma B_k B_k^T) - 2(C_k\Gamma C_k + \Gamma C_k\Gamma)) \\ & = C_k + \Gamma + \frac{1}{2}(C_k\Gamma - \Gamma C_k) - \frac{1}{12}(B_k B_k^T \Gamma + \Gamma B_k B_k^T) + \mathcal{O}(\|C_k\|^i \|\Gamma\|^j) \end{aligned}$$

where $i, j \geq 1$ are placeholders for any combination of indices with $i + j = 3$. Ignoring the quadratic terms $\Gamma C_k, C_k\Gamma$ and the higher ones and setting to zeros yields a symmetric Sylvester equation for Γ :

$$(19) \quad C_k = S_k\Gamma + \Gamma S_k, \quad \text{with } S_k := \left(\frac{1}{12} B_k B_k^T - \frac{1}{2} I_p \right).$$

A sufficient criterion that guarantees a unique solution is that $\|B_k\|_2 < \sqrt{6}$, since in this case $\frac{1}{6}\|B_k B_k^T\|_2 < 1$, which entails that all eigenvalues of S_k are strictly negative. This in turn yields that S_k and $-S_k$ have disjoint spectra, which ensures the unique solvability of (19), [7, Section VII.2]. When selecting Γ_k as the solution to (19) at each iteration k , then the lower p -by- p diagonal block of the BCH series cancels up to fourth order commutator terms and terms that are quadratic in C_k and Γ_k .

Remark 6. This choice does not cancel all terms that are of first order in Γ in the BCH series of $\log_m(V_kW)$. The series is ordered by the degree of nested commutators brackets. In the j th-order commutator term, “words” formed by j “letters” of the two-letter alphabet $\{\log_m(V_k), \log_m(W)\}$ appear, where each of $\log_m(V_k), \log_m(W)$ appears at least once, see [37, 26, 39]. This means that no matter where we cut off the tail of the BCH series, there remain terms that are linear in $\|\Gamma\|$ (or $\|C_k\|$ for that matter). Expanding the series for $\log_m(V_kW)$ in powers of W as in [25, Section 8.1] will not solve the issue, because the collection of all terms that are of first order in $\|W\|$ constitutes an infinite series by itself that needs to be truncated in numerical applications.

Experiments show that this choice of Γ_k at every iteration step of [40, Alg. 1] improves the iteration count by a factor of 2 and accelerates the algorithm by a factor of 1.5. In the algorithm, we introduce a Boolean “Flag_Sylv on/off” to switch between the original version [40, Alg. 1] and the “Sylvester-enhancement”. A detailed convergence analysis can be conducted as in [40] but is not worthwhile in the context of this work. However, the next proposition allows to compare the asymptotic convergence rate of Algorithm 4 with “Flag_Sylv” off, which is the original method [40, Alg. 1] that employs $\Gamma = -C_k$ for the update, and Algorithm 4 with “Flag_Sylv” on, which then computes Γ from (19).

Algorithm 4 Improved algebraic Stiefel logarithm, canonical metric ($\alpha = 0$).

Input: $U, \tilde{U} \in St(n, p)$, $\epsilon > 0$ convergence threshold, Boolean “Flag_Sylv on/off”

- 1: $M := U^T \tilde{U} \in \mathbb{R}^{p \times p}$
- 2: $QN := \tilde{U} - UM \in \mathbb{R}^{n \times p}$ {compact QR-decomp.}
- 3: $V_0 := \begin{pmatrix} M & X_0 \\ N & Y_0 \end{pmatrix} \in O_{2p \times 2p}$ {orthogonal completion}
- 4: **for** $k = 0, 1, 2, \dots$ **do**
- 5: $\begin{pmatrix} A_k & -B_k^T \\ B_k & C_k \end{pmatrix} := \log_m(V_k)$ {matrix log, A_k, C_k skew}
- 6: **if** $\|C_k\|_2 \leq \epsilon$ **then**
- 7: **break**
- 8: **end if**
- 9: **if** Flag_Sylv **then**
- 10: $S_k := \frac{1}{12} B_k B_k^T - \frac{1}{2} I_p$
- 11: solve $C_k = S_k \Gamma + \Gamma S_k$ for Γ {sym. Sylvester equation}
- 12: **else**
- 13: $\Gamma := -C_k$ {cancel first term in BCH series}
- 14: **end if**
- 15: $\Phi_k := \exp_m(\Gamma)$ {matrix exp, Φ_k orthogonal}
- 16: $V_{k+1} := V_k W_k$, where $W_k := \begin{pmatrix} I_p & 0 \\ 0 & \Phi_k \end{pmatrix}$ {update}
- 17: **end for**

Output: $\Delta := \text{Log}_U^{St}(\tilde{U}) = U A_k + Q B_k \in T_U St(n, p)$

PROPOSITION 7. *Suppose that the input data $U \neq \tilde{U} \in St(n, p)$ are such that Algorithm 4 converges with “Flag_Sylv” on. Assume further that there is a bound $0 < \delta < 1$ such that for $\log_m(V_k) = \begin{pmatrix} A_k & -B_k^T \\ B_k & C_k \end{pmatrix}$, it holds $\|\log_m(V_k)\|_2 < \delta$ throughout the algorithm’s iteration loop.² Then, for k large enough, it holds*

$$\|C_{k+1}\|_2 \leq \left(\frac{6}{6 - \delta^2} \frac{\delta^4}{1 - \delta} + \mathcal{O}(\|C_k\|_2) \right) \|C_k\|_2.$$

This implies the asymptotic convergence rate of Algorithm 4 with “Flag_Sylv” on for $k \rightarrow \infty$. This compares to the asymptotic rate of [40, Alg. 1], which according to [40, eq. (12)] is bounded by

$$\|C_{k+1}\|_2 \leq \left(\frac{1}{6} \delta^2 + \frac{\delta^4}{1 - \delta} + \mathcal{O}(\|C_k\|_2) \right) \|C_k\|_2.$$

Proof. Since $\|B_k\|_2 \leq \|\log_m(V_k)\| < \delta < 1$, the matrices $S_k = \frac{1}{12} B_k B_k^T - \frac{1}{2} I_p$ are negative definite with largest eigenvalue bounded by $-\frac{1}{2} + \frac{\delta^2}{12} = -\frac{6 - \delta^2}{12}$. Hence, the spectra of the symmetric matrices S_k and $-S_k$ are separated by a vertical strip of width $\frac{6 - \delta^2}{6}$ in the complex plain. Applying [7, Theorem VII.2.12] to the Sylvester equation $S_k \Gamma + \Gamma(-S_k) = C_k$ yields $\|\Gamma\|_2 \leq \frac{6}{6 - \delta^2} \|C_k\|_2$. Calculating C_{k+1} according to (18) but with this choice of Γ shows that all terms up to order four in the BCH

²For the original Stiefel log algorithm, conditions for the existence of such a global bound δ are established in [40, Lemma 4.4]. Similar techniques apply in this context.

series are at least quadratic in $\|C_k\|_2$:

$$\begin{aligned} C_{k+1} &= \frac{1}{2}[C_k, \Gamma] + \frac{1}{12}([C_k^2, \Gamma] + [C_k, \Gamma^2]) - 2(C_k \Gamma C_k + \Gamma C_k \Gamma) \\ &\quad + \frac{1}{24}([B_k B_k^T, \Gamma^2] - (C_k^2 \Gamma^2 + \Gamma^2 C_k^2) + 2[C_k \Gamma C_k, \Gamma]) + \text{h.o.t.}(5), \end{aligned}$$

where h.o.t.(5) are the terms of fifth order and higher in the BCH series. From $U \neq \tilde{U}$, we get $\lim_{k \rightarrow \infty} \begin{pmatrix} A_k & -B_k^T \\ B_k & C_k \end{pmatrix} \neq 0$. Hence, for k large enough, it holds $\|\Gamma\|_2 \leq \frac{6}{6-\delta^2} \|C_k\|_2 \leq \left\| \begin{pmatrix} A_k & -B_k^T \\ B_k & C_k \end{pmatrix} \right\|_2 = \|\log_m(V_k)\|_2$. Because C_{k+1} is but the lower diagonal subblock of $\log_m(V_k W)$, the higher-order terms are bounded by $\|\text{h.o.t.}(5)\|_2 \leq \sum_{l=5}^{\infty} \|\log_m(V_k)\|_2^{l-1} \|\Gamma\|_2 \leq \frac{6}{6-\delta^2} \|C_k\|_2 \frac{\delta^4}{1-\delta}$, see [40, Lemma A.1]. The claim is now a straightforward consequence. \square

Proposition 7 shows that with smaller values of δ , the Sylvester approach becomes more and more favorable. The actual value of δ depends on how close the inputs U, \tilde{U} are. For $\delta \approx 0.7147$ the bounds for the asymptotic convergence rates are the same for both the approaches ‘‘Flag_Sylv on/off’’; for $\delta \approx 0.3286$ the rate of the Sylvester-based method is improved a factor of 2 and by a factor of 10 for $\delta \approx 0.1270$. Note that in both cases, the bounds overestimate the true convergence rates.

The main computational effort of **Algorithm 4** is in the computation of the matrix logarithm in step 5. This can be achieved efficiently (and without resorting to complex numbers arithmetics) by first computing a real Schur form. Assuming that the principal matrix logarithm is properly defined, the Schur form of an orthogonal matrix is block-diagonal with blocks (1) of size (1×1) and blocks of the form $\begin{pmatrix} \cos(\varphi) & -\sin(\varphi) \\ \sin(\varphi) & \cos(\varphi) \end{pmatrix}$, the matrix logarithm of such a block being $\begin{pmatrix} 0 & -\varphi \\ \varphi & 0 \end{pmatrix}$. This is exploited in the actual implementation.

3.5. A geodesic Newton method for the Stiefel logarithm. The nonlinear matrix equation (14) can be cast in the following form

$$V^T F \begin{pmatrix} A & -B^T \\ B & C \end{pmatrix} = I, \quad \text{where } V = \begin{pmatrix} M & X_0 \\ N & Y_0 \end{pmatrix} \in SO(2p).$$

For brevity, introduce

$$\hat{F} : \text{skew}(2p) \rightarrow SO(2p), \quad S \mapsto V^T F(S).$$

The parameter domain $\text{skew}(2p)$ has a vector space structure that allows to employ Euclidean techniques. The co-domain, however is the Lie group $SO(2p)$. Ignoring the structure of $SO(2p)$, the classical Newton method can be applied to the root finding problem $V^T F(S) - I = 0$. Given a starting point S_0 , Newton requires to solve the Taylor-linearized problem

$$I = \hat{F}(S) + D\hat{F}_S(H) \approx \hat{F}(S + H)$$

so that the update H is determined by the linear system $D\hat{F}_S(H) = I - \hat{F}(S)$. Yet, the left-hand side and the right-hand side are not compatible, as $\hat{F}(S) \in SO(2p)$ and $D\hat{F}_S(H) \in T_{\hat{F}(S)} SO(2p) = \hat{F}(S) \text{skew}(2p)$.

A remedy is to replace the Euclidean first-order Taylor approximation, which can be thought of as progressing along a straight line, by moving along a geodesic

in the same direction. This leads to a first-order approximation that preserves the Riemannian structure

$$\hat{F}(S + H) \approx \text{Exp}_{\hat{F}(S)}(D\hat{F}_S(H)).$$

On $SO(2p)$, the geodesic that starts from $\hat{F}(S)$ in the direction $D\hat{F}_S(H)$ is

$$\text{Exp}_{\hat{F}(S)}(D\hat{F}_S(H)) = \hat{F}(S) \exp_m(\hat{F}(S)^T D\hat{F}_S(H)),$$

see e.g. [14]. The first-order approximation to (14) becomes

$$(20) \quad \begin{aligned} I &= \hat{F}(S) \exp_m(\hat{F}(S)^T D\hat{F}_S(H)) \\ \Leftrightarrow \underbrace{\hat{F}(S)^T D\hat{F}_S(H)}_{\text{skew}} &= \underbrace{\log_m(\hat{F}(S)^T)}_{\text{skew}}. \end{aligned}$$

The left-hand side is a linear operator

$$L_S : \text{skew}(2p) \rightarrow \text{skew}(2p), \quad H \mapsto \hat{F}(S)^T D\hat{F}_S(H).$$

In summary, this leads to the iterative scheme stated in [Algorithm 5](#). Upon conver-

Algorithm 5 GeoNewton for solving (14)

- 1: $k = 0$
 - 2: **while** $\|\log_m(\hat{F}(S_k)^T)\|_{\text{fro}} > \tau$ **do**
 - 3: solve $L_{S_k}(H_k) = \log_m(\hat{F}(S_k)^T)$
 - 4: update $S_{k+1} = S_k + H_k$
 - 5: $k = k + 1$
 - 6: **end while**
-

gence, $S_k = \begin{pmatrix} A_k & -B_k^T \\ B_k & C_k \end{pmatrix}$ is found and the output $\Delta := \text{Log}_U^{St}(\tilde{U}) = U A_k + Q B_k \in T_U$ is formed with U, Q as in [Algorithm 4](#). Computationally, the expensive part is to evaluate the operator L_S . For convenience, let us restrict to the Euclidean metric and write

$$S = \begin{pmatrix} A & -B^T \\ B & C \end{pmatrix}, \quad S_{\text{tri}} = \begin{pmatrix} 2A & -B^T \\ B & 0 \end{pmatrix}, \quad S_{\text{di}} = \begin{pmatrix} A & 0 \\ 0 & C \end{pmatrix},$$

likewise for $H \in \text{skew}(2p)$. It holds

$$(21) \quad \begin{aligned} L_S(H) &= \hat{F}(S)^T D\hat{F}_S(H) = F(S)^T V V^T D F_S(H) \\ &= F(S)^T (D(\exp_m)_{S_{\text{tri}}}(H_{\text{tri}}) \exp_m(-S_{\text{di}}) + \exp_m(S_{\text{tri}}) D(\exp_m)_{S_{\text{di}}}(-H_{\text{di}})). \end{aligned}$$

In an implementation, we do not actually form this operator, but implement its action on a matrix H . This is then used in a matrix-free version of the GMRES algorithm [32] (as pre-installed in Matlab, version R2019b). For the practical evaluation of $D(\exp_m)_S(H)$, we use Mathias' Theorem [15, Thm 3.6], which simultaneously gives $\exp_m(S)$.

An equivalent alternative to (14) is to solve

$$(22) \quad 0 = \log_m(F(S)) - \log_m(V).$$

In this form, both the unknown S and the output $\log_m(F(S)) - \log_m(V)$ are in the vector space $\text{skew}(2p)$ so that this equation is amenable to be treated with the classical

Newton method. However, computing or approximating the derivative remains the computational bottleneck. The associated linear operator now involves differentials of both the matrix exponential and the matrix logarithm. We tackle this with the same strategy as above by relying on Mathias' Theorem and the matrix-free GMRES method. The matrix functions $\exp_m(S)$ and $\log_m(S)$ may be approximated with via the Cayley transformation $\text{Cay}(S) = (I - \frac{1}{2}S)^{-1}(I + \frac{1}{2}S)$ and its inverse; likewise the differentials of $D(\exp_m)_S(H)$ and $D(\log_m)_S(H)$ may be approximated with the differentials of the corresponding Cayley transformations.

We mention these approaches for the sake of completeness and include the algorithms based on (20) and (22) in the algorithmic competition. However, the numerical experiments show that none of the above approaches can compete neither with the p -shooting method Algorithm 2 nor with the algebraic Stiefel log algorithm Algorithm 4. This also holds, when the Cayley transformations are used to replace \exp_m and \log_m . Therefore, we omit a detailed discussion.

4. Numerical experiments. In this section, we perform numerical experiments for assessing the performance of the various approaches to solve the local geodesic endpoint problem. All experiments are performed with Matlab R2019b on a Linux 64bit HP notebook with four Intel(R) Core(TM) i7-5600U 2.60GHz CPUs.

4.1. First experiment: the geodesic endpoint problem for the canonical metric. We create two points U, \tilde{U} pseudo-randomly on $St(n, p)$, but such that they are a prescribed distance apart. More precisely, we construct U from a QR-decomposition of a random $(n \times p)$ -matrix with entries sampled from the uniform distribution. Then, we create a random tangent vector $\Delta = UA + (I - UU^T)T$, where $A \in \mathbb{R}^{p \times p}$ is random but skew and $T \in \mathbb{R}^{n \times p}$ is random. Then, Δ is scaled to the prescribed length according to the Riemannian metric and $\tilde{U} \in St(n, p)$ is obtained as $\tilde{U} = \text{Exp}_U(\Delta)$.

Then, the various Stiefel-log algorithms are applied to reconstruct the tangent vector and the absolute accuracy is checked in the infinity-matrix norm. In summary, we perform the following three steps

$$(a) \quad \tilde{U} = \text{Exp}_U(\Delta), \quad (b) \quad \Delta_{rec} = \text{Log}_U(\tilde{U}), \quad (c) \quad \|\Delta - \Delta_{rec}\|_\infty.$$

We perform 10 runs with random data, record the numerical accuracy, the iteration count and the computation time and average over the results. In order to evaluate the logarithm, we use the following methods:

- Alg. 4 as in [40].
- Alg. 4 enhanced by the Sylvester equation (19) as detailed in Subsection 3.4.
- Alg. 4 enhanced by (19) and with the Cayley transformation replacing the matrix exponential in Step 15.
- Alg. 2 on two time steps $\{0.0, 1.0\}$ in the unit interval $[0, 1]$.
- Alg. 2 on four time steps $\{0.0, 0.3, 0.6, 1.0\}$ of the unit interval $[0, 1]$.

In each case, the convergence threshold is set to $\tau = 10^{-11}$. Table 1 displays the results for data on $St(n = 2000, p = 500)$ with $\text{dist}(U, \tilde{U}) = 5\pi$, for data on $St(n = 120, p = 30)$ with $\text{dist}(U, \tilde{U}) = \pi$ and for data on $St(n = 12, p = 3)$ with $\text{dist}(U, \tilde{U}) = 0.95\pi$. Observe that in all cases, the data exceed the estimated injectivity radius of $St(n, p)$, which is at least 0.89π and most likely not larger, see [29]. Example plots of the convergence histories are shown in Figure 2 and Figure 3, respectively.

The table shows that Algorithm 4 with ‘‘Flag_Sylv’’ on exhibits the best performance for the cases considered, both in terms of the numerical accuracy and the

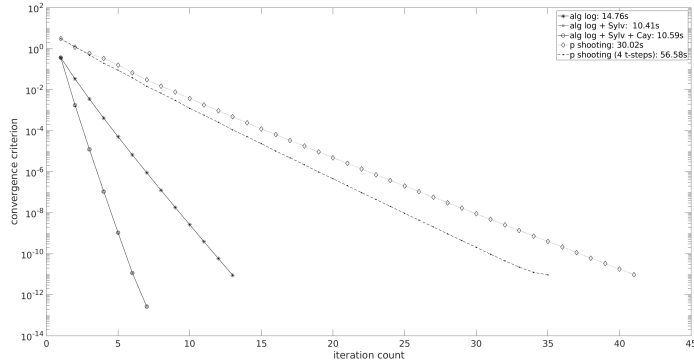


FIG. 2. *Convergence history of the various log-algorithms for computing $\text{Log}_U(\tilde{U})$ for the canonical metric. The graphs show one one run of the test case $St(2000, 500)$. The input data is at a Riemannian distance of $\text{dist}(U, \tilde{U}) = 5\pi$*

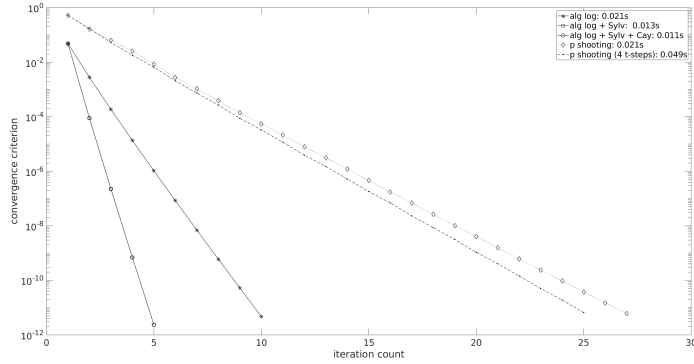


FIG. 3. *Convergence history of the various log-algorithms for computing $\text{Log}_U(\tilde{U})$ for the canonical metric. The graphs show one one run of the test case $St(120, 30)$. The input data is at a Riemannian distance of $\text{dist}(U, \tilde{U}) = 1\pi$*

computation time. It can also be seen that a subdivision of the interval $[0, 1]$ is not required for [Algorithm 2](#) in order to converge for the larger data sets under consideration. The dimensions and distance for the low-dimensional data set on $St(12, 3)$ are chosen as in [\[36\]](#), where the global geodesic endpoint problem is considered. In fact, the methods considered here are local by nature, however, they still converge in some cases, while they diverge in other cases, see [Table 1](#) for details. The p-shooting method on four time steps in $[0, 1]$ converges in all cases considered, while it diverges in all cases, if only the boundary points of $[0, 1]$ are considered in the discrete parallel transport.

4.2. Second experiment: the geodesic endpoint problem for the Euclidean metric. In this section, we repeat the experiments of [Subsection 4.1](#) with exactly the same set-up, but for the Euclidean metric. Since the algebraic Stiefel log algorithm [Alg. 4](#) is not available for metrics other than the canonical one, we juxtapose the following methods

- [Alg. 5](#), “GeoNewton”, the geodesic Newton method for [\(14\)](#)
- [Alg. “EucNewton”](#), based on the classical Newton method for solving [\(22\)](#).
- [Alg. 2](#) on two time steps $\{0.0, 1.0\}$ of the unit interval $[0, 1]$.

(Sec. 4.1) Test Case 1: random data $n = 2000$, $p = 500$, canonical metric, 10 runs			
$\text{dist}(U, \tilde{U}) = 5\pi$			
Method	av. rel. error $\ \Delta - \Delta_{rec}\ _\infty$	av. iter. count	av. time
Alg. 4	$0.41 \cdot 10^{-11}$	13.0	14.76s
Alg. 4 + Sylv.	$0.018 \cdot 10^{-11}$	7.0	10.41s
Alg. 4 + Sylv. + Cayley	$0.018 \cdot 10^{-11}$	7.0	10.60s
Alg. 2 on 2 steps	$0.49 \cdot 10^{-11}$	41.1	30.02s
Alg. 2 on 4 steps	$0.34 \cdot 10^{-11}$	35.1	56.58s

(Sec. 4.1) Test Case 2: random data $n = 120$, $p = 30$, canonical metric, 10 runs			
$\text{dist}(U, \tilde{U}) = \pi$			
Method	av. rel. error $\ \Delta - \Delta_{rec}\ _\infty$	av. iter. count	av. time
Alg. 4	$0.215 \cdot 10^{-11}$	10.2	0.021s
Alg. 4 + Sylv.	$0.138 \cdot 10^{-11}$	5.0	0.013s
Alg. 4 + Sylv. + Cayley	$0.139 \cdot 10^{-11}$	5.0	0.011s
Alg. 2 on 2 steps	$0.291 \cdot 10^{-11}$	26.8	0.021s
Alg. 2 on 4 steps	$0.225 \cdot 10^{-11}$	24.4	0.049s

(Sec. 4.1) Test Case 3: random data $n = 12$, $p = 3$, canonical metric, 100 runs			
$\text{dist}(U, \tilde{U}) = 0.95\pi$ (averaging only over the converged runs)			
Method	av. rel. error $\ \Delta - \Delta_{rec}\ _\infty$	av. iter. count	av. time
Alg. 4	$0.342 \cdot 10^{-10}$ (*62 runs not conv'd)	88.3	0.045s
Alg. 4 + Sylv.	$0.155 \cdot 10^{-10}$ (*31 runs not conv'd)	50.6	0.033s
Alg. 4 + Sylv. + Cayley	$0.157 \cdot 10^{-10}$ (*31 runs not conv'd)	50.8	0.026s
Alg. 2 on 2 steps	(*all 100 runs not conv'd)	–	–
Alg. 2 on 4 steps	$0.606 \cdot 10^{-10}$ (*all 100 runs conv'd.)	212.2	0.033s

TABLE 1
Numerical performance for the cases considered in [Subsection 4.1](#)

• Alg. 2 on four time steps $\{0.0, 0.\bar{3}, 0.\bar{6}, 1.0\}$ of the unit interval $[0, 1]$. In each case, the convergence threshold is set to $\tau = 10^{-11}$. [Table 2](#) displays the results for data on $St(n = 120, p = 30)$ with $\text{dist}(U, \tilde{U}) = \pi$ and for data on $St(n = 2000, p = 500)$ with $\text{dist}(U, \tilde{U}) = 5\pi$. In the latter case, only one random run is performed due to the large computation times for the Newton methods. Example plots of the convergence histories are shown in [Figure 4](#) and [Figure 5](#), respectively.

The table shows that [Algorithm 2](#) without a subdivision of $[0, 1]$ exhibits the best performance in terms of the computation time for the cases considered here. For the larger test case, the method is 60–70 times faster than the Newton-based methods and also much more memory efficient. These computation times are representative for other values of α in the family of Riemannian metrics.

4.3. Third experiment: the Riemannian barycenter of geodesic Stiefel triangles. As a last test case, we compute the Riemannian center of mass of a geodesic triangle on $St(n, p)$. The Riemannian center of mass for centers w.r.t. a general mass distribution is investigated in [\[20\]](#) and is occasionally referred to as the Fréchet mean; also the misnomer “Karcher mean” [\[21\]](#) is in use. Here, we need the concept only for discrete, finite point sets. For fixed points $\{U_0, \dots, U_k\} \in St(n, p)$ and scalar weights $w_i \leq 0$, $\sum_{i=0}^k w_i = 1$, the center of mass is defined as the mini-

(Sec. 4.2) Test Case 1: random data $n = 2000$, $p = 500$, Euclidean metric, 1 run $\text{dist}(U, \tilde{U}) = 5\pi$			
Method	rel. error $\ \Delta - \Delta_{rec}\ _\infty$	iter. count	time
Alg. GeoNewton	$0.403 \cdot 10^{-11}$	13	1025.6s
Alg. EucNewton	$0.0438 \cdot 10^{-11}$	6	884.4s
Alg. 2 on 2 steps	$0.287 \cdot 10^{-11}$	20	14.70s
Alg. 2 on 4 steps	$0.151 \cdot 10^{-11}$	11	18.23s

(Sec. 4.2) Test Case 2: random data $n = 120$, $p = 30$, Euclidean metric, 10 runs $\text{dist}(U, \tilde{U}) = \pi$			
Method	av. rel. error $\ \Delta - \Delta_{rec}\ _\infty$	av. iter. count	av. time
Alg. GeoNewton	$0.754 \cdot 10^{-12}$	8.0	0.351s
Alg. EucNewton	$0.165 \cdot 10^{-12}$	5.0	0.882s
Alg. 2 on 2 steps	$0.631 \cdot 10^{-12}$	13.1	0.0115s
Alg. 2 on 4 steps	$0.119 \cdot 10^{-12}$	9.0	0.0222s

TABLE 2
Numerical performance for the cases considered in Subsection 4.2

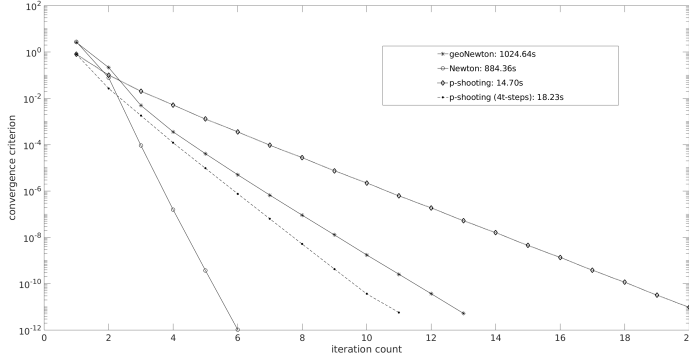


FIG. 4. Convergence history of the various log-algorithms for computing $\text{Log}_U(\tilde{U})$ for the Euclidean metric. The graphs show one run of the test case $St(2000, 500)$. The input data is at a Riemannian distance of $\text{dist}(U, \tilde{U}) = 5\pi$

mizer(s) of the Riemannian objective function

$$(23) \quad St(n, p) \ni U \mapsto f(U) = \frac{1}{2} \sum_{i=0}^k w_i \text{dist}(U, U_i)^2,$$

where $\text{dist}(U, U_i)$ is the Riemannian distance between U, U_i corresponding to the selected metric. On curved manifolds, the global center might not be unique. Moreover, local minimizers may appear. For more details, see [20] and [3]. The latter reference also states uniqueness criteria.

The simplest approach to minimizing (23) is a gradient descent method [3, 2]. The gradient of the objective function f in (23) is

$$(24) \quad \nabla f_U = - \sum_{i=0}^k w_i \text{Log}_U(U_i) \in T_U St(n, p),$$

see [20, Thm 1.2], [3, §2.1.5], [33, eq. (2.4)]. Hence, multiple evaluations of the Riemannian logarithm map are required to compute the gradient, which makes the

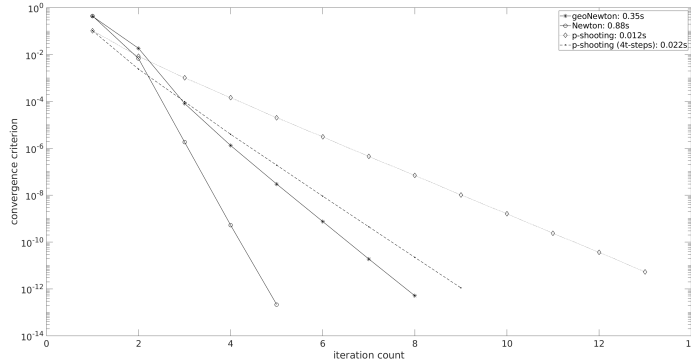


FIG. 5. Convergence history of the various log-algorithms for computing $\text{Log}_U(\tilde{U})$ for the Euclidean metric. The graphs show one one run of the test case $St(120, 30)$. The input data is at a Riemannian distance of $\text{dist}(U, \tilde{U}) = 1\pi$

problem computationally more challenging. Generic gradient descent algorithms are considered in [30, 3], we restate the basic method in Algorithm 6.

Algorithm 6 Weighted Riemannian center, [30, 3]

Input: Data set $\{U_0, \dots, U_k\} \subset St(n, p)$, initial guess U_0^* , convergence threshold τ .

- 1: $j := 0$
- 2: Compute $\nabla f_{U_j^*}$ according to (24)
- 3: **while** $\|\nabla f_{U_j^*}\| > \tau$ **do**
- 4: select a step size $\delta_j > 0$
- 5: $U_{j+1}^* := \text{Exp}_{U_j^*}(-\delta_j \nabla f_{U_j^*})$
- 6: $j := j + 1$
- 7: **end while**

Output: Center point $U^* := U_j^*$.

Experimental set-up. In order to create a geodesic triangle, we start with $U_0 \in St(n, p)$ selected randomly as outlined in Subsection 4.1. The corner points U_1 and U_2 are constructed such that $\text{dist}(U_0, U_1) = \text{dist}(U_0, U_2) = 0.8\pi$. In this way, an *isosceles triangle* is obtained, see Figure 6 for a stylized illustration. For our basic performance experiment, we use equal weights $w_0 = w_1 = w_2 = \frac{1}{3}$ and conduct Algorithm 6 with a fixed step size $\delta_j = \delta = 0.5$. The convergence threshold for the gradient descent is set to $\tau = 10^{-10}$.

For obtaining the logarithm, we use the methods that proved to perform the fastest in the previous sections, namely Algorithm 4 with the Sylvester-enhancement and Algorithm 2. The convergence threshold for each Riemannian log evaluation is $\tau = 10^{-11}$. Table 3 lists the associated number of iterations and computation times for $n = 1100$ and increasing dimensions $p \in \{200, 300, 400, 500\}$. Both methods produce the same Riemannian center in the same number of gradient search iterations. For $p = 200, 300$, Algorithm 2 is faster than its competitor, but is overtaken by Algorithm 4 for $p = 400, 500$. Both methods prove to be reliable tools for the Riemannian log calculations within this optimization task.

5. Conclusions and final remarks. We have presented a unified formula for the geodesics on the Stiefel manifold for a one-parameter family of Riemannian met-

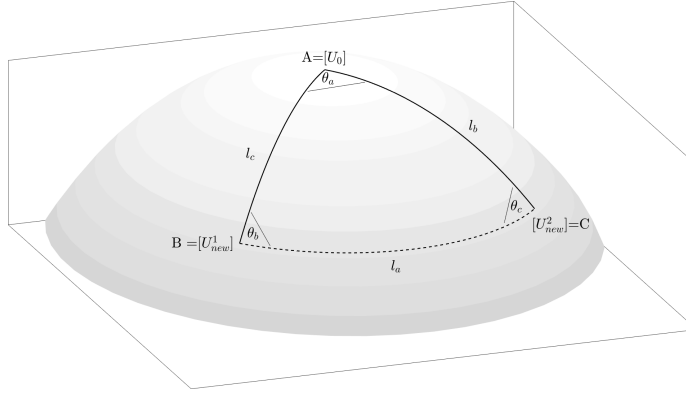


FIG. 6. Schematic picture of a geodesic triangle on a manifold. The sides \overline{AB} and \overline{AC} have the same lengths l_c, l_b by construction. We use a gradient descent to compute the Riemannian center of mass.

(Sec. 4.3) Riemannian center of geodesic triangle	
Data dimension $(n, p) = (1100, 200)$	
Method	time
Alg. 4 + Sylv + Cay	35.71s
Alg. 2 on 2 steps	33.35s
Data dimension $(n, p) = (1100, 300)$	
Method	time
Alg. 4 + Sylv + Cay	100.73s
Alg. 2 on 2 steps	93.85s
Data dimension $(n, p) = (1100, 400)$	
Method	time
Alg. 4 + Sylv + Cay	174.53s
Alg. 2 on 2 steps	196.05s
Data dimension $(n, p) = (1100, 500)$	
Method	time
Alg. 4 + Sylv + Cay	310.61s
Alg. 2 on 2 steps	369.04s

TABLE 3

Numerical performance for the cases considered in Subsection 4.3.

rics. The formula combines the benefits of the separate formulas known for the Euclidean metric and the canonical metric from the literature: (1) It works with $(n \times p)$ -matrices as representatives in numerical schemes; (2) it requires the matrix exponential for structured, skew-symmetric matrices. variety of methods for computing the Stiefel log.

Starting from the unified geodesic formula, we have derived a unified non-linear matrix equation that is associated with the geodesic endpoint problem and thus the Riemannian logarithm. We have shown that the formula also holds for rank-deficient tangent vectors and observed that the computations can be essentially restricted to finding certain rotations that scale in the dimension p but are independent of n . Based on this fact, we customized the shooting method of [8] to work essentially on the small matrix factors, which we termed p -shooting method. This method works for all α -metrics. Moreover, we introduced an enhancement to the Riemannian loga-

rithm of [40] that is specific to the canonical metric. As possible alternatives, we mentioned Newton-based methods. However, in the numerical experiments the p -shooting method and the enhanced algebraic algorithm outperformed their competitors. Both methods worked efficiently for computing the Riemannian center of a geodesic triangle in a Stiefel manifold of comparably large dimensions.

The methods developed in this paper address the *local* geodesic endpoint problem. Yet, the experiments show, that they converge occasionally also for data sets that are well beyond the estimated injectivity radius of the Stiefel manifold.

REFERENCES

- [1] P.-A. Absil, R. Mahony, and R. Sepulchre. Riemannian geometry of Grassmann manifolds with a view on algorithmic computation. *Acta Applicandae Mathematica*, 80(2):199–220, 2004.
- [2] P.-A. Absil, R. Mahony, and R. Sepulchre. *Optimization Algorithms on Matrix Manifolds*. Princeton University Press, Princeton, New Jersey, 2008.
- [3] B. Afsari, R. Tron, and R. Vidal. On the convergence of gradient descent for finding the Riemannian center of mass. *SIAM Journal on Control and Optimization*, 51(3):2230–2260, 2013.
- [4] E. Begelfor and M. Werman. Affine invariance revisited. *IEEE Conference on Computer Vision and Pattern Recognition*, 2:2087–2094, 2006.
- [5] P. Benner, S. Gugercin, and K. Willcox. A survey of projection-based model reduction methods for parametric dynamical systems. *SIAM Review*, 57(4):483–531, 2015.
- [6] A. V. Bernstein and A. P. Kuleshov. Tangent bundle manifold learning via Grassmann & Stiefel eigenmaps. *arXiv preprint arXiv:1212.6031*, 2012.
- [7] R. Bhatia. *Matrix Analysis*. Number 169 in Graduate Texts in Mathematics. Springer-Verlag, New York – Berlin – Heidelberg, 1997.
- [8] D. Bryner. Endpoint geodesics on the Stiefel manifold embedded in Euclidean space. *SIAM Journal on Matrix Analysis and Applications*, 38(4):1139–1159, 2017.
- [9] E. Celledoni, S. Eidesnes, B. Owren, and T. Ringholm. *Mathematics of Computation*, (89):699–716, 2020.
- [10] R. Chakraborty and B. C. Vemuri. Statistics on the (compact) Stiefel manifold: Theory and applications. *arXiv:1708.00045v1*, 2017.
- [11] M. P. do Carmo. *Riemannian Geometry*. Mathematics: Theory & Applications. Birkhäuser Boston, 1992.
- [12] A. Edelman, T. A. Arias, and S. T. Smith. The geometry of algorithms with orthogonality constraints. *SIAM Journal on Matrix Analysis and Applications*, 20(2):303–353, April 1998.
- [13] K. A. Gallivan, A. Srivastava, X. Liu, and P. Van Dooren. Efficient algorithms for inferences on Grassmann manifolds. In *IEEE Workshop on Statistical Signal Processing*, pages 315–318, 2003.
- [14] R. Godement and U. Ray. *Introduction to the Theory of Lie Groups*. Universitext. Springer International Publishing, 2017.
- [15] N. J. Higham. *Functions of Matrices: Theory and Computation*. Society for Industrial and Applied Mathematics, Philadelphia, PA, USA, 2008.
- [16] K. Hüper, M. Kleinstüber, and F. Silva Leite. Rolling Stiefel manifolds. *International Journal of Systems Science*, 39(9):881–887, 2008.
- [17] K. Hüper, I. Markina, and F. Silva Leite. A Lagrangian approach to extremal curves on Stiefel manifolds. *Journal of Geometrical Mechanics*, 13(1):55–72, 2021.
- [18] K. Hüper and F. Ullrich. Real Stiefel manifolds: An extrinsic point of view. In *2018 13th APCA International Conference on Automatic Control and Soft Computing (CONTROL)*, pages 13–18, June 2018.
- [19] A. Iserles, H. Z. Munthe-Kaas, S. P. Nørsett, and A. Zanna. Lie-group methods. *Acta Numerica*, 9:215–365, 2000.
- [20] H. Karcher. Riemannian center of mass and mollifier smoothing. *Communications on Pure and Applied Mathematics*, 30(5):509–541, 1977.
- [21] H. Karcher. Riemannian center of mass and so called Karcher mean. *arXiv:1407.2087v1*, 2014.
- [22] J. M. Lee. *Riemannian Manifolds: an Introduction to Curvature*. Springer Verlag, New York – Berlin – Heidelberg, 1997.
- [23] J. M. Lee. *Introduction to Riemannian Manifolds*. Graduate Texts in Mathematics. Springer International Publishing, Cham, 2018.

- [24] Y. Man Lui. Advances in matrix manifolds for computer vision. *Image and Vision Computing*, 30(6–7):380–388, 2012.
- [25] M. Müger. Notes on the theorem of Baker-Campbell-Hausdorff-Dynkin. 2019.
- [26] M. Newman, S. Wasin, and R. C. Thompson. Convergence domains for the Campbell-Baker-Hausdorff formula. *Linear and Multilinear Algebra*, 24(4):301–310, 1989.
- [27] L. Noakes. A global algorithm for geodesics. *Journal of the Australian Mathematical Society. Series A. Pure Mathematics and Statistics*, 65(1):37–50, 1998.
- [28] I. U. Rahman, I. Drori, V. C. Stodden, D. L. Donoho, and P. Schröder. Multiscale representations for manifold-valued data. *SIAM Journal on Multiscale Modeling and Simulation*, 4(4):1201–1232, 2005.
- [29] Q. Rentmeesters. *Algorithms for data fitting on some common homogeneous spaces*. PhD thesis, Université Catholique de Louvain, Louvain, Belgium, 2013.
- [30] Q. Rentmeesters and P.-A. Absil. Algorithms comparison for Karcher mean computation of rotation matrices and diffusion tensors. In *Proceedings of the 19th European Signal Processing Conference (EUSIPCO 2011)*, Barcelona, Spain, Aug. 29 - Sept. 2 2011.
- [31] W. Rossmann. *Lie Groups: An Introduction Through Linear Groups*. Oxford Graduate Texts in Mathematics. Oxford University Press, 2006.
- [32] Youcef Saad and Martin H Schultz. Gmres: A generalized minimal residual algorithm for solving nonsymmetric linear systems. *SIAM J. Sci. Stat. Comput.*, 7(3):856–869, 1986.
- [33] O. Sander. Geodesic finite elements of higher order. *IMA Journal of Numerical Analysis*, 36(1):238–266, 2016.
- [34] A. Srivastava and E. P. Klassen. *Functional and Shape Data Analysis*. Springer Series in Statistics. Springer Verlag, New York, 2016.
- [35] Ganesh Sundaramoorthi, Andrea Mennucci, Stefano Soatto, and Anthony Yezzi. A new geometric metric in the space of curves, and applications to tracking deforming objects by prediction and filtering. *SIAM Journal on Imaging Sciences*, 4(1):109–145, 2011.
- [36] M. Sutti and B. Vandereycken. The leapfrog algorithm as nonlinear Gauss–Seidel. arXiv:2010.14137v1, 2020.
- [37] R. C. Thompson. Convergence proof for Goldberg’s exponential series. *Linear Algebra and its Applications*, 121:3–7, 1989.
- [38] P. K. Turaga, Veeraraghavan A., and R. Chellappa. Statistical analysis on Stiefel and Grassmann manifolds with applications in computer vision. In *2008 IEEE Conference on Computer Vision and Pattern Recognition*, pages 1–8, June 2008.
- [39] A. Van-Brunt and M. Visser. Simplifying the Reinsch algorithm for the Baker-Campbell-Hausdorff series. arXiv:1501.05034, 2015.
- [40] R. Zimmermann. A matrix-algebraic algorithm for the Riemannian logarithm on the Stiefel manifold under the canonical metric. *SIAM Journal on Matrix Analysis and Applications*, 38(2):322–342, 2017.
- [41] R. Zimmermann. Manifold interpolation and model reduction. arXiv:1902.06502v1, 2019.
- [42] R. Zimmermann. Hermite interpolation and data processing errors on Riemannian matrix manifolds. *SIAM Journal on Scientific Computing*, 42(5):A2593–A2619, 2020.
- [43] R. Zimmermann. Manifold interpolation. In P. Benner, S. Grivet-Talocia, A. Quarteroni, G. Rozza, W. Schilders, and L. M. Silveira, editors, *System- and Data-Driven Methods and Algorithms*, volume 1 of *Model Order Reduction*. De Gruyter, Boston, 2021.